

Effects of correlated interactions in a biological coevolution model with individual-based dynamics

Volkan Sevim¹ and Per Arne Rikvold^{1,2}

¹ School of Computational Science, Center for Materials Research and Technology, and Department of Physics, Florida State University, Tallahassee, FL 32306-4120, USA

² National High Magnetic Field Laboratory, Tallahassee, FL 32310-3706, USA

E-mail: sevim@csit.fsu.edu, rikvold@csit.fsu.edu

Abstract. Models of biological coevolution have recently been proposed and studied, in which a species is defined by a genome in the form of a finite bitstring, and the interactions between species i and j are given by a fixed matrix with independent, randomly distributed elements M_{ij} . A consequence of the stochastic independence is that species whose genotypes differ even by a single bit may have completely different phenotypes, as defined by their interactions with the other species. This is clearly unrealistic, as closely related species should be similar in their interactions with the rest of the ecosystem. Here we therefore study a model, in which the M_{ij} are correlated to a controllable degree by means of a local averaging scheme. We calculate, both analytically and numerically, the correlation function for matrix elements M_{ij} and M_{kl} versus the Hamming distance between the bitstrings representing the species. The agreement between the analytical and numerical calculations is excellent for correlations of limited range, but explainable differences arise for correlation ranges that are a significant fraction of the length of the bitstring. We compare long kinetic Monte Carlo simulations of coevolution models with uncorrelated and correlated interactions, respectively. In particular, we consider the probability density for the lifetimes of individual species. The species-lifetime distribution is close to a power law with an exponent near -2 over eight decades in time in both uncorrelated and correlated cases. The durations of quasi-steady states and power spectral densities for the diversity indices display noticeable differences. However, some qualitative features, like $1/f$ behaviour in power spectral densities for the diversity indices, are not affected by the correlations in the interaction matrix.

PACS numbers: 87.23.Kg, 05.40.-a, 05.65.+b, 89.75.-k

Submitted to: *Physical Biology*

1. Introduction

During the last decade, ecological dynamics and biological evolution have become new areas of interest for statistical physicists [1]. This trend has merged with recent developments in the theory of complex networks [2], which has drawn increased attention to problems in ecological dynamics, such as the evolution and stability of food webs [1, 3, 4, 5, 6].

While many models of macroevolution are formulated explicitly at evolutionary (macroscopic) time scales, evolutionary dynamics in nature are driven by reproduction, mutations, and selection at the ecological (microscopic) scale of individual organisms. Although this means that individual-based models of macroevolution must span a dauntingly large range of timescales, this is now becoming possible with the aid of modern computers and algorithms. We therefore recently studied an individual-based biological coevolution model [7, 8, 9] with random interspecies interactions. This model is a simplified version of the tangled-nature model introduced by Jensen, *et al.* [10, 11, 12]. Individuals are represented by a haploid genome consisting of a string of bits. The individuals reproduce asexually and interact with individuals of other species through a random interaction matrix with stochastically independent elements, which determine how the reproduction probability of individuals of each species is affected by the presence and abundance of other species in the “ecosystem”. During reproduction, an offspring individual can randomly mutate with a small but constant probability by having a single bit in its genome flipped. These mutations create perturbations in the ecosystem by introducing new species. A particular mutant may or may not succeed, depending on its interactions with the species already present in the system. Usually a mutant does not fit in well with the resident species, and so it quickly goes extinct. However, occasionally a successful mutant can cause avalanches of mass extinctions, destroying some or all of the other species through predation or competition. As a consequence, the individuals in this model ecosystem live in a dynamic “fitness landscape”, which evolves due to changes in the populations of the resident species and the introduction of new species through mutations. The model displays quiet periods interrupted by bursts of high activity caused by mass extinctions that are triggered by the introduction of new mutants, reminiscent of the punctuated-equilibrium mode of evolution suggested by Eldredge and Gould [13, 14, 15]. The lifetime distribution for individual species is well described by a power law with exponent close to -2 .

A rather unrealistic aspect of this model is the fact that the elements of the interaction matrix are completely uncorrelated. This means that a mutant in general will have completely different interactions with other species, and thus a completely different phenotype, than does its parent “wildtype”. In the present paper, we therefore modify our previous model by introducing correlations into the interaction matrix. (Similar ideas have been pursued by Kauffman [16, 17].) In the modified model, the correlations between matrix elements ensure that mutants are not completely different from their parents. Rather, their interactions with the other species are similar to those of the

wildtype. The price to be paid is a significant reduction in the number of effectively independent phenotypes for a genome of a given length. In this paper we compare numerical results for this modified model with results for the corresponding uncorrelated model in order to assess the effects of including correlations. The results show that, although long-range correlations affect the dynamics of the system noticeably, some qualitative features remain unchanged.

The organization of the rest of this paper is as follows. In section 2 we describe the model and the algorithm used for the simulations. In section 3 we describe the construction of the correlated interaction matrix and briefly discuss some complications of this process. In section 4 we report our results, which are summarized in section 5. Derivations of our analytical results are provided in the Appendices.

2. Model

A species in our Monte Carlo (MC) simulations is represented by a bitstring genome of length L . This L -bit genome supplies a pool of 2^L possible species. These organisms are considered haploids. Thus, the terms “species”, “species index”, and “genotype” are synonymous in this paper.

Individuals in the simulation are allowed to give birth to F offspring per generation with a probability P_i , where i denotes the species index. The reproduction is asexual (cloning), and it occurs in discrete, nonoverlapping generations. Thus, only offspring can survive to the next generation, and all individuals die at the end of the generation whether they reproduce or not. We use a mathematically convenient, nonlinear form for the probability of reproduction [7, 8, 10, 11, 18], given by

$$P_i(\{n_j(t)\}) = \frac{1}{1 + \exp \left[- \sum_j M_{ij} n_j(t) / N_{\text{tot}}(t) + N_{\text{tot}}(t) / N_0 \right]}, \quad (1)$$

where $n_i(t)$ is the population of species i at time t . The Verhulst factor N_0 represents the carrying capacity of the “ecosystem” and keeps the total population, $N_{\text{tot}}(t) = \sum_i n_i(t)$, finite. \mathbf{M} is the interaction matrix, in which a matrix element M_{ij} represents the effect of the population density of species j on species i . Species i benefits from species j if M_{ij} is positive, and it is inhibited by species j if M_{ij} is negative. There is no interaction between species i and j when M_{ij} is zero. The structure of \mathbf{M} is discussed in the next section.

Although we begin the simulations with a population consisting of only one species, the system diversifies quickly because, in each generation, all individuals are exposed to mutations that create new species. The mutation process is modelled by flipping a randomly chosen bit in the individual’s genome with a probability μ per generation per individual.

We note that the population dynamics used in the model is somewhat unrealistic, due to the absence of external energy resources and conservation of energy (or biomass) [7, 8, 9, 10, 11, 12].

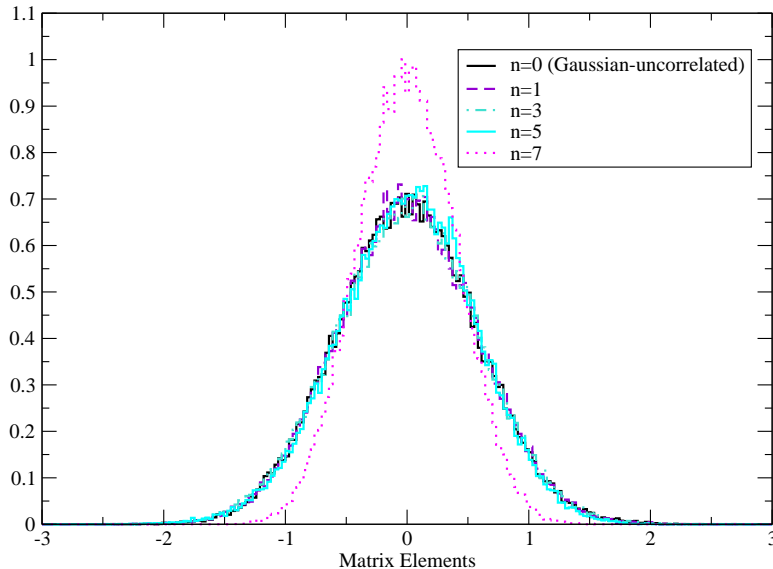


Figure 1. Some realizations of matrix-element distributions for typical runs with $L = 8$ and $n = 0, 1, 3, 5,$ and 7 . (The distributions are *not* averaged over independent runs.) For these particular realizations, the distributions for $n = 0, 1, 3,$ and 5 practically overlap. The distribution for $n = 7$ is narrower due to effects that are explained in section 3.2.

3. The Interaction Matrix

3.1. Form of the Matrix

The structure of the interaction matrix characterizes the dynamics of the system. Rikvold and Zia [7, 8] studied the same system (except for a negligible probability of $O(\mu^2)$ for multiple mutations) using an interaction matrix with off-diagonal elements distributed randomly and uniformly over $[-1, 1]$ and with the diagonal elements set to zero. We shall call this the uniform-uncorrelated model. For reasons that will become clear later, we instead use a Gaussian distribution to facilitate some comparisons. We call this model the Gaussian-uncorrelated (or just the uncorrelated) model.

The main focus of this paper is the effects of correlations in the interaction matrix. (Some preliminary results of this work were discussed in reference [18].) The motivation behind the introduction of correlations is the following. In reality, the interaction between two species x and z should be positively correlated with the interaction between species y and z if x and y are closely related. Therefore, one would expect a positive correlation between the matrix elements M_{xz} and M_{yz} .

A correlated matrix is generated using the following method. First, a random matrix with elements drawn from a Gaussian distribution with standard deviation $\sigma_0 = \sqrt{1/3}$ and mean zero is generated. (We chose this standard deviation for backward compatibility with earlier studies in which the matrix elements were uniformly distributed on $[-1, 1]$.) Then, each matrix element in the random matrix is averaged over itself and its neighbours in genome space up to a Hamming distance n , where

n is the averaging radius. Thus, the total number of terms in the average (or the number of points inside the averaging “hypersphere” with radius n in genome space) is $Z_n = \sum_{m=0}^n \binom{2L}{m}$. The average is multiplied by $\sqrt{Z_n}$ in order to keep the standard deviation of the correlated matrix elements approximately the same as for the random ones. This process eliminates any possible effect by a change in the shape of the distribution of interaction strengths. Thus, a correlated matrix element M_{ij} is given by

$$M_{ij} = \sum_{H(ij;kl) \leq n} M_{kl}^0 / \sqrt{Z_n}, \quad (2)$$

where M_{kl}^0 are the elements of the uncorrelated matrix, which are Gaussian distributed with standard deviation σ_0 , and $H(ij;kl)$ is the Hamming distance between two matrix elements M_{ij}^0 and M_{kl}^0 . We use the city-block metric to define the Hamming distance between two matrix elements. Therefore, $H(ij;kl) = H(i,k) + H(j,l)$, where $H(i,j)$ is the Hamming distance between bitstrings i and j . In fact, $H(ij;kl)$ denotes the Hamming distance between the concatenated bitstrings ij and kl . (This concatenation notation is useful for Hamming distance calculations and will be used throughout the paper.) The diagonals are set to zero *after* the averaging process is finished. The model in which such a correlated interaction matrix is used is called the correlated model. Theoretical calculations of correlation functions are discussed in Appendix A.

There are two modelling issues that need to be discussed here. The first one is the interpretation of the mutation process. As we mentioned above, in the uncorrelated model, matrix elements M_{xz}^0 and M_{yz}^0 are not correlated, even if y is a mutant of x . (We call y a mutant of x if $H(x,y) = 1$.) Therefore, the set of interactions between the mutant y and other species can be completely different than those between the wildtype x and the other species. This lack of relationship between the mutant and the wildtype is not very realistic. Therefore, the mutation process in the uncorrelated model may, in some sense, be interpreted as the introduction of a completely new species to the system from a pool of species, reminiscent of migration. In the correlated model, the interaction constants of the mutant and the wildtype are correlated. However, whether these correlations are strong enough to describe those between a real mutant and its wildtype is arguable. The other issue is the non-antisymmetrical form of \mathbf{M} , meaning $M_{ij} \neq -M_{ji}$. This feature of the model, along with the absence of an external energy source, gives rise to unrealistic numbers of mutualistic interactions in the system [7].

We have already made a preliminary comparison between the correlated model and the Gaussian- and uniform-uncorrelated models in reference [18] for short-range correlations, $n = 1$ and $n = 2$. The results suggested that the correlated and Gaussian-uncorrelated models behave quite similarly, so that short-range correlations in \mathbf{M} may not have a significant effect on the dynamics. In this paper, we extend our investigation to the effects of longer-range correlations with $n > 2$.

3.2. Distributions of Matrix Elements, Correlations Between Matrix Elements, and Complications in the Averaging Process

The averaging process mentioned above causes a few unexpected complications. The first one is a shift in the mean. Although the matrix elements are drawn from a distribution with mean zero, for a finite matrix, the mean, $\langle M_{ij}^0 \rangle$, while quite small, is always non-zero. The averaging alters the mean of the matrix elements, so that the means of the initial random and the averaged matrices can be considerably different. The reason for the shift is the following. Since each averaged element is multiplied by $\sqrt{Z_n}$ to keep the standard deviation constant, the mean of the elements of the averaged interaction matrix becomes $\langle M_{ij} \rangle = \sqrt{Z_n} \langle M_{ij}^0 \rangle$. Although $\langle M_{ij}^0 \rangle$ is a negligibly small number, multiplication by a large $\sqrt{Z_n}$ could cause a considerable shift, $\langle M_{ij} \rangle - \langle M_{ij}^0 \rangle$, in the mean. In order to prevent this, we adjust the mean, $\langle M_{ij}^0 \rangle$, by subtracting $\langle M_{ij}^0 \rangle / 2^{2L}$ from each element of the initial random matrix. This modification minimizes the shift in the mean.

The other complication of the averaging process is a change in the standard deviation of M_{ij} , even though we intend to keep it constant. As in the problem of the shift in the mean mentioned above, the standard deviation of the averaged matrix can be considerably different than that of the initial random matrix. As seen in figure 1, the matrices averaged for $n = 1$ have approximately the same Gaussian form with a standard deviation close to σ_0 , which practically overlaps with the M_{ij}^0 distribution of the initial Gaussian-uncorrelated matrix. However, we found that long-range averaging ($n \gtrsim L/2$) could generate distributions with significantly different standard deviations, like the $n = 7$ curve included in figure 1. The reason for the change in the standard deviation is very similar to that for the shift in the mean mentioned above. This anomaly is discussed further in Appendix B.

We also checked the correlations between matrix elements to see the effect of averaging. The correlations between two matrix elements, M_{ij} and $M_{i'j'}$, depend on the overlap of the M_{kl}^0 terms that occur in the average in equation (2). Theoretical calculations predict decaying correlation functions with steps due to the city-block metric, as shown in figure A1. These calculations are explained in Appendix A.

The correlation functions of the matrices with short-range correlations are in good agreement with the theory. However, as n is increased, the numerical correlation functions begin to deviate from their theoretical counterparts, as shown in figure 2. The numerical correlation functions of the highly correlated matrices are distorted and translated along the y -axis, compared to the theoretical ones. We believe that the cause of this anomaly is related to the cause of the anomaly in the standard deviations. This complication is discussed in Appendix B.

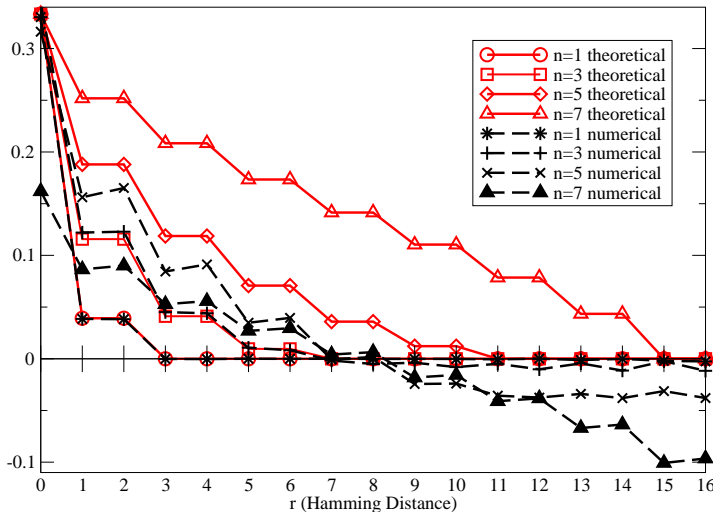


Figure 2. Theoretical and some numerical realizations of correlation functions between matrix elements as functions of the Hamming distance between their indices, $r = H(ij, kl)$, with $L = 8$; $n = 1, 3, 5,$ and 7 . The numerical correlation functions were not averaged over independent realizations in order to show the magnitudes and the character of the deviations. Theory and numerics agree for small n . Increasing n leads to deviations from the theory, usually retaining the overall shape of the expected correlation function. (Numerical calculations were performed before setting the diagonal of \mathbf{M} to zero.)

4. Simulation Results

Unless otherwise indicated, we performed sixteen independent runs for $2^{25} = 33\,554\,432$ generations for each model using parameters similar to those in references [7] and [18]: genome length $L = 8$ bits, mutation rate $\mu = 10^{-3}$ per individual per generation, carrying capacity $N_0 = 2000$, fecundity $F = 4$; and for the correlated model, averaging radii $n = 1, 3, 5,$ and 7 . Each run used a different \mathbf{M} and a different sequence of random numbers. Each simulation started with 200 individuals of genotype 0. The system parameters were recorded every sixteen steps.

In order to see the effect of the shape of the M_{ij}^0 distribution, we first ran four sets of simulations of the uncorrelated model with a uniform M_{ij}^0 distribution with standard deviation σ_0 , and with a Gaussian M_{ij}^0 distribution with standard deviations $\sigma_0/2$, σ_0 and $2\sigma_0$. For these systems with different M_{ij}^0 distributions, we compared histograms of species lifetimes. The species lifetime is defined as the number of generations between creation and extinction of a species, during which its population is continuously positive.

As seen in figure 3, the lifetime distributions of the uncorrelated systems with different matrix-element distributions all exhibit approximately power-law like decay over seven decades in time, with an exponent near -2 . Figure 3 also shows that a narrower M_{ij}^0 distribution flattens the concavity between 10 and 10^4 generations in the lifetime distribution, while a wider one makes it deeper.

The lifetime distributions of the correlated models shown in figure 4 also exhibit a

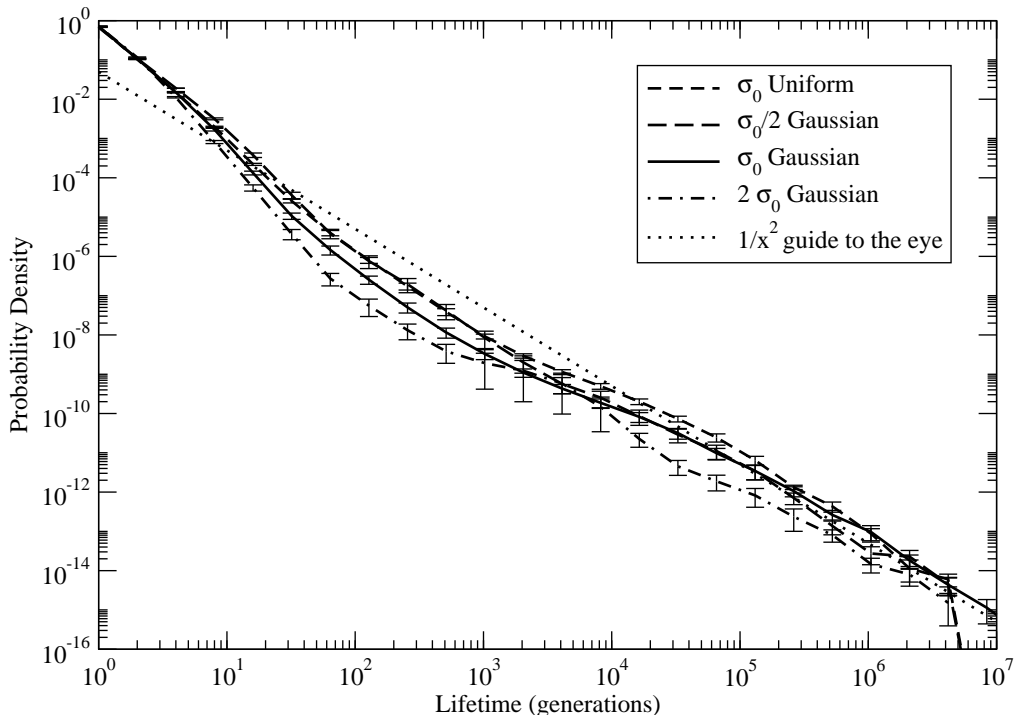


Figure 3. Normalized histograms of species-lifetimes for the uncorrelated model with a uniform matrix-element distribution with standard deviation σ_0 , and with Gaussian matrix-element distribution widths, $\sigma_0/2$, σ_0 , and $2\sigma_0$. Based on simulations of 2^{25} generations each with $L = 8$, averaged over eight runs.

power-law like decay similar to the ones in figure 3. The distributions obtained from the simulations with very short-range correlations, like $n = 1$, practically overlap with the one corresponding to the uncorrelated model. Increasing n leads to a deviation from the distribution of the uncorrelated model. The $n = 3, 5$, and 7 curves in figure 4 look similar to the $\sigma_0/2$ curve in figure 3, suggesting that the change in the standard deviation (or the shape) of the M_{ij} distribution could perhaps be responsible for this anomaly. In order to make sure that it is actually the correlations that cause the changes, we suppressed this anomaly: we ran another set of simulations for $n = 7$ in which the standard deviation of the M_{ij} distribution was adjusted to σ_0 after averaging. The result is shown in the inset in figure 4. The two lifetime distributions in the inset almost completely coincide. They are both the averages of eight-run sets with $n = 7$ (using the same random number sequences), except that the M_{ij} distribution of the second set is adjusted after averaging. The very small difference between these two curves shows that the effect of a change in the standard deviation of the M_{ij} distribution after averaging is negligible. Thus, the correlations in \mathbf{M} are largely responsible for the differences between the lifetime distributions of the correlated and uncorrelated models, shown in the main part of figure 4.

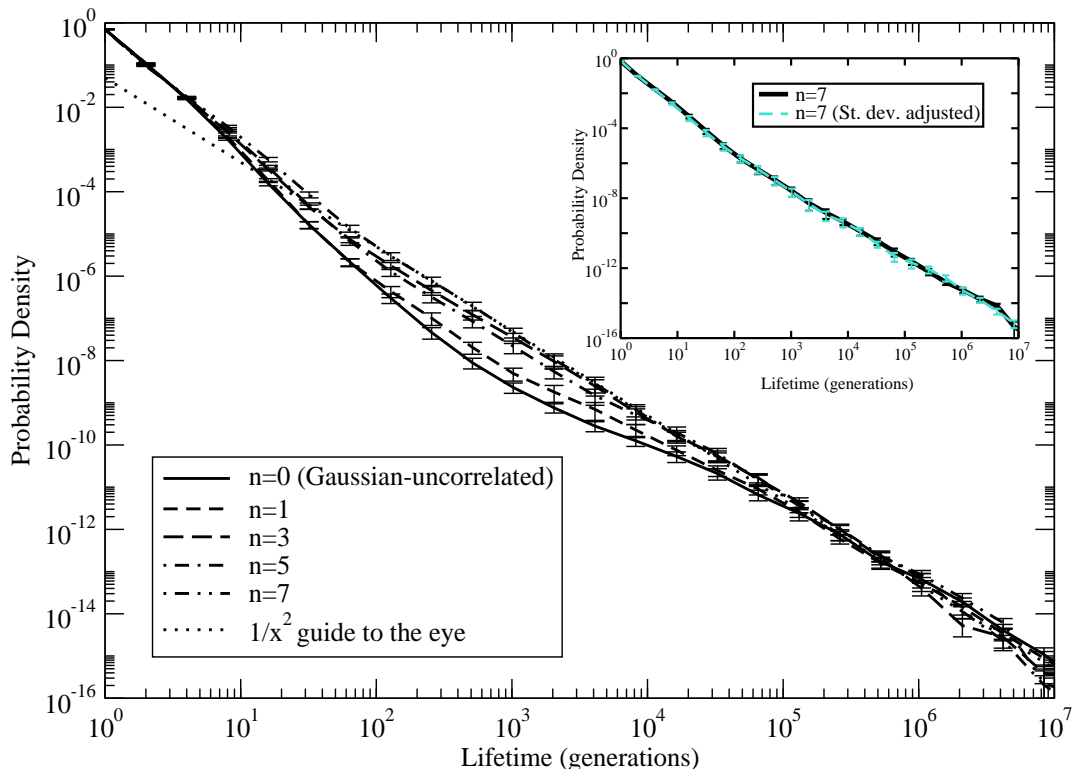


Figure 4. Normalized histograms of species lifetimes for uncorrelated and correlated models with different averaging radii, based on simulations of 2^{25} generations each with $L = 8$. Each curve represents an average over sixteen runs. The standard deviations of the M_{ij} distributions change after averaging. The averages of the new standard deviations are 0.5755(6), 0.570(3), 0.54(1), and 0.46(1) for $n = 1, 3, 5,$ and 7 , respectively, compared to $\sigma_0 = 0.5773$. Inset: The lifetime histograms for $n = 7$ with and without adjusting the standard deviation of the M_{ij} , averaged over eight runs each. The same sets of random numbers were used for the “adjusted” eight-run set as for their “non-adjusted” counterparts. The distributions practically overlap, suggesting that the change in the standard deviation has much less effect on the lifetime distribution than the correlations in \mathbf{M} .

The deviation trend in the lifetime distributions is not monotonic in the averaging radius (the $n = 5$ curve appears below the $n = 3$ curve). However, the error bars for the $n = 3$ and $n = 5$ curves overlap. The large error margin due to the anomaly in the correlation functions leaves some uncertainty. Nevertheless, even fairly long-range correlations in \mathbf{M} (like $n = 5$ and 7) do not change the gross features like the approximate $1/t^2$ behaviour of the lifetime distributions.

Another set of statistical measurements that we made for the durations of the quasi-steady states (QSS) gave a somewhat conflicting result. The QSSs are the metastable periods, during which the community structure appears to be stationary [7, 8]. They are interrupted by active periods, during which the community structure changes after the emergence of a successful mutant and resulting extinction of other species. In order to identify the QSSs, we recorded the entropy of the system every sixteen generations.

The information-theoretical entropy is given by [19, 20],

$$S(\{n_I(t)\}) = - \sum_{\{I|\rho_I(t)>0\}} \rho_I(t) \ln \rho_I(t) , \quad (3)$$

where $\rho_I(t) = n_I(t)/N_{\text{tot}}(t)$. The system is considered in a QSS, as long as the magnitude of the entropy difference, $|S(t) - S(t - 16)|/16$, is below a certain threshold, which we took as 0.015. (For an extensive discussion on how to obtain this value, see reference [7].) The QSS-duration distribution for the uncorrelated model is not significantly affected by the change in the standard deviation of the M_{ij} distribution, except the density of the longest lived communities around 10^7 generations (figure 5(a)). Considering the large error bars at this range, the QSS distributions of the uncorrelated systems nearly overlap. However, the correlations in \mathbf{M} seem to increase the lifetimes of the QSS communities (figure 5(b)).

In order to get more information on how the fluctuations in the system are affected by the correlations in \mathbf{M} , we also calculated the power spectral density (PSD) of the Shannon-Wiener diversity index. The Shannon-Wiener diversity index [21] is defined as $D(t) = \exp[S(\{n_I(t)\})]$, where S is the information-theoretical entropy defined in equation (3). In contrast to the QSS statistics (figure 5(a)) (but consistent with the case for the species-lifetime, figure 4), the PSDs of the Shannon-Wiener indices of the uncorrelated systems with different M_{ij} distributions do not overlap (figure 6(a)) [22, 23]. Although the PSDs are not monotonic in the standard deviation of M_{ij} , they have a similar $1/f$ like shape, indicating that the general characteristics of the system do not vary significantly with the M_{ij} distribution. However, the correlations in \mathbf{M} lead to a more pronounced $1/f$ like behaviour in the PSDs by increasing the relative weight of high-frequency fluctuations as the correlations grow stronger (figure 6(b)). Although the deviations from the uncorrelated case are neither gradual nor monotonic in correlation strength, the result suggests that the correlations in \mathbf{M} may in fact change some characteristics of the system, supporting the result obtained from the QSS duration statistics. Nevertheless, the qualitative $1/f$ behaviour of the PSDs is not affected by these changes.

The results discussed above may seem rather complicated, but we nevertheless believe some clear effects can be discerned.

There are clear differences between the results for the correlated and uncorrelated Gaussian matrix elements. The correlations further increase the proportion of very long QSS (figure 5b), but curiously they also lead to an increase of intermediate-lifetime species (figure 4). These effects do not seem very easy to reconcile, but we speculate that they may be due to a decoupling of the species lifetimes and the QSS durations that has been observed in an uncorrelated predator-prey version of this model [9]. The increased activity in the intermediate-time regime results in increased intensity in the higher-frequency half of the PSD (figure 6b). It should be noted that strong correlation effects are only seen when n becomes a significant proportion of the genome length L (here, typically $n \geq 3$). Such long-range correlations are of very limited interest for the biological systems, and they only become significant in the present study because we,

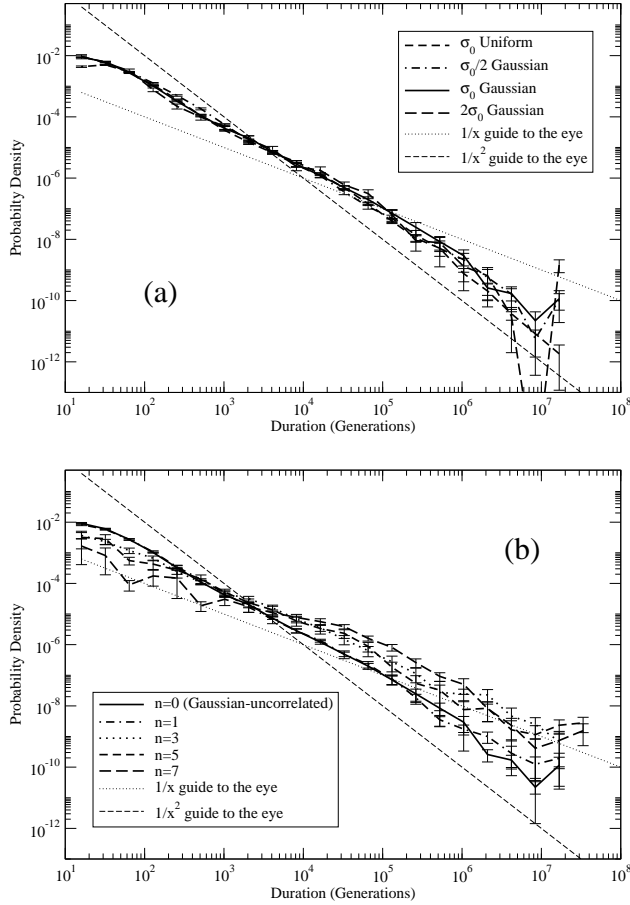


Figure 5. Normalized histograms for the duration of quasi-steady states. A cut-off of $|S(t) - S(t - 16)|/16 = 0.015$ was used to distinguish between QSS and active periods. Each curve represents an average over eight runs for uncorrelated models and sixteen runs for correlated models. Based on simulations of 2^{25} generations each, sampled every sixteen generations. (a) Simulations for uncorrelated models with uniform and Gaussian M_{ij} distributions with the standard deviations σ_0 , and $\sigma_0/2$, σ_0 , and $2\sigma_0$, respectively. The distributions are very similar for the uncorrelated model. (b) Simulations for the uncorrelated and the correlated models with $n = 1, 3, 5$, and 7 . The Gaussian σ_0 and the $n = 0$ curves are identical. The distributions for the correlated systems differ from the uncorrelated one.

for computational reasons, are working with the unrealistically short genome length, $L = 8$. With $n \ll L$, the effects of correlations appear to be quite minor.

5. Summary and Conclusions

In this paper we have considered the effects of introducing correlations between the elements of the interaction matrix \mathbf{M} that determines the interspecies interactions in an individual-based coevolution model [7, 8, 9], in which individuals are represented by a genome in the form of a bitstring of length L .

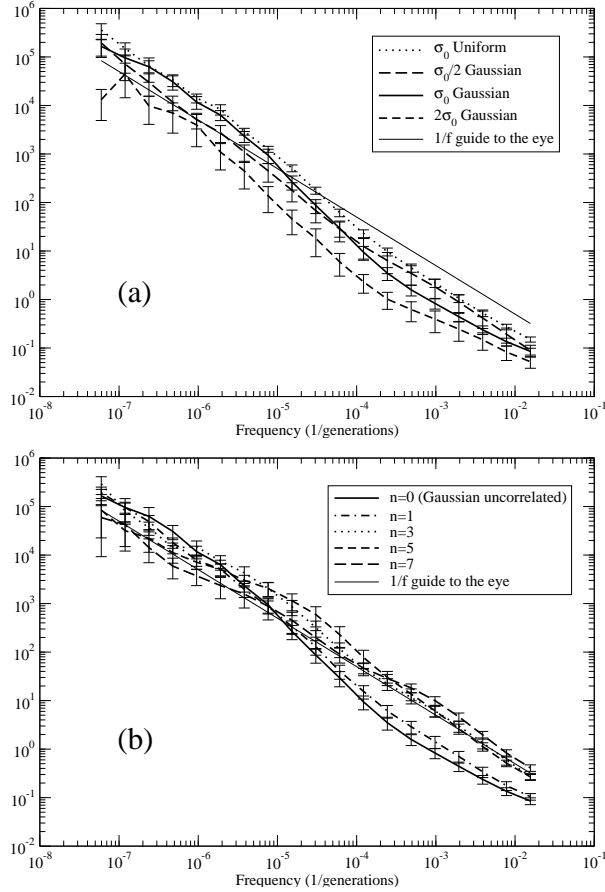


Figure 6. Power spectral densities of Shannon-Wiener diversity indices for different models. Each curve represents an average over eight runs for the uncorrelated models and sixteen runs for the correlated models. Based on simulations of 2^{25} generations each, sampled every sixteen generations. The results obtained from each run were also averaged over each octave to reduce the noise. (a) Simulations for uncorrelated models with uniform and Gaussian M_{ij} distributions with the standard deviations σ_0 , and $\sigma_0/2$, σ_0 , and $2\sigma_0$, respectively. (b) Simulations for uncorrelated and correlated models with $n = 1, 3, 5$, and 7 . The Gaussian σ_0 and the $n = 0$ curves are identical. The distributions for the correlated systems differ slightly from the uncorrelated one.

The correlations were introduced by replacing each element M_{ij}^0 in an uncorrelated interaction matrix with the average over all the elements M_{kl}^0 such that the Hamming distance between the concatenated bitstrings ij and kl is less than or equal to n , and then reweighting the resulting matrix element M_{ij} such as to maintain the standard deviation of its probability density unchanged.

In section 3 we calculated numerically for different n the correlation functions between modified matrix elements M_{ij} and M_{kl} as functions of the Hamming distance between ij and kl , and we compared these with the theoretical results derived in Appendix A. For short-range correlations ($n < L/2$) we found good agreement between the numerical and theoretical results, but for larger n there were significant

discrepancies. These discrepancies were explained in Appendix B as a result of the reweighting of the correlated matrix elements that was performed in order to keep their standard deviation approximately equal to that of the uncorrelated ones.

Next, in section 4, we performed long kinetic Monte Carlo simulations of our coevolution model, both with correlated and uncorrelated interaction matrices. As an indicator of the similarity of the evolution processes we calculated the probability densities of the lifetimes of individual species in the two models. While we found statistically significant differences between the lifetime distributions in the two models (see figure 4), in both cases the distributions stayed near a $1/t^2$ power law over near seven decades in time. However, the distributions for the durations of QSSs (figure 5) and the PSDs for the diversity index (figure 6) showed that the uncorrelated and correlated systems have some different characteristics. Nevertheless, the overall behaviour of the system does not seem to change drastically, since the $1/f$ behaviour in the PSDs remain the same. This indicates that the correlations in \mathbf{M} affect the long-term behaviour of the system in minor, but rather complicated ways. The correlation effects are sufficiently mild that it is permissible to draw conclusions from simulations of uncorrelated models.

Acknowledgments

We thank G. Brown, D. T. Robb, S. Frank, and R. K. P. Zia for helpful comments. This research was supported by U.S. National Science Foundation Grant Nos. DMR-0240078 and DMR-0444051, and by Florida State University through the School of Computational Science, the Center for Materials Research and Technology, and the National High Magnetic Field Laboratory.

Appendix A. Calculating the Correlation Function

The correlations between elements of the interaction matrix are described by the correlation function $C(r) = \langle M_{ij}M_{kl} \rangle_r - \langle M_{ij} \rangle \langle M_{kl} \rangle$. The subscript r means that the averages are not calculated over all matrix elements, but only over ones that are separated by a Hamming distance $H(ij; kl) = r$. Assuming the average of the matrix elements, $\langle M_{ij} \rangle$, is zero, the correlation function simply becomes

$$C(r) = \langle M_{ij}M_{kl} \rangle_r . \quad (\text{A.1})$$

Substituting equation (2) into equation (A.1) gives

$$\langle M_{ij}M_{kl} \rangle_r = Z_n^{-1} \left\langle \sum_{\rho \leq n} M_{ab}^0 \sum_{\rho' \leq n} M_{cd}^0 \right\rangle_r , \quad (\text{A.2})$$

where $\rho = H(ij; ab)$ and $\rho' = H(kl; cd)$. By expanding the sums in the average, we obtain

$$\langle M_{ij}M_{kl} \rangle_r = \langle (M_{ab}^0 + M_{a'b'}^0 + \dots)(M_{cd}^0 + M_{c'd'}^0 + \dots) \rangle / Z_n . \quad (\text{A.3})$$

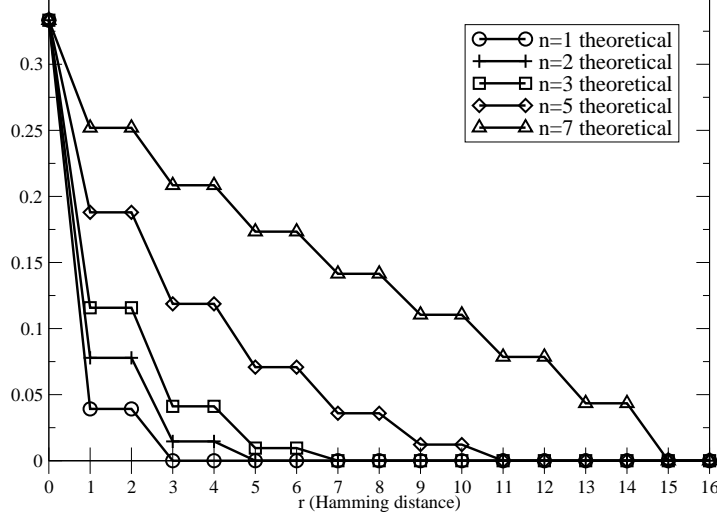


Figure A1. Theoretical correlation functions for $L = 13$ with $n = 1, 2, 3, 5,$ and 7 .

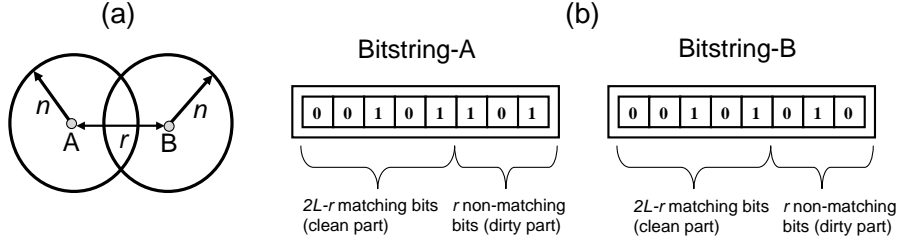


Figure A2. (a) Common elements in the two sums shown symbolically as the intersection of two $2L$ -dimensional hyperspheres in genome space with radii n . (b) “Dirty” and “clean” parts. See discussion in the text.

In this average, all cross terms, $\langle M_{ab}^0 M_{cd}^0 \rangle$ where $a \neq c$ and/or $b \neq d$, are equal to zero. However, if $a = c$ and $b = d$, then the term $\langle (M_{ab}^0)^2 \rangle$ is equal to σ_0^2 , which is the variance of the elements of the random interaction matrix. Therefore, the correlation function becomes

$$C(r) = \langle M_{ij} M_{kl} \rangle_r = \mathcal{N}_{L,n}(r) \sigma_0^2 / Z_n = \mathcal{N}_{L,n}(r) / 3Z_n, \quad (\text{A.4})$$

where $\mathcal{N}_{L,n}(r)$ is the number of common terms in the two sums in equation (A.2). The calculation of $\mathcal{N}_{L,n}(r)$ is explained below.

Appendix A.1. Calculating $\mathcal{N}_{L,n}(r)$

The terms in the sum in equation (2) are neighbours of M_{ij}^0 within a hypersphere of “radius” n , centred at ij in the $2L$ -dimensional genome space. So, the common terms in the sums in equation (A.2) are the ones which lie in the intersection of two $2L$ -dimensional “hyperspheres” of radii n , centred at $A = ij$ and $B = kl$ (figure A2(a)). This analogy helps us to reformulate the problem of finding the common terms in the

sums in equation (A.2) as the following. What is the total number of bitstrings that are n bits or less away from both bitstrings A and B , when A and B differ from each other by r bits? Equivalently, we want to find the number of identical bitstrings we can create by making n or less modifications on A and B each.

To make it easier to visualize the solution, we arrange the two bitstrings A and B so that the matching bits constitute the left-hand part of each bitstring. We shall call these $2L - r$ matching bits the *clean part*, and the r non-matching bits the *dirty part* (figure A2(b)). We emphasize that this arrangement is only for visualization purposes, and not a part of the solution.

The contributions to $\mathcal{N}_{L,n}(r)$ can be grouped in three cases:

- a) $n \geq r \geq 0$: First, we make the dirty parts identical by making i modifications on either A or B and $r - i$ modifications on the other. There are $\sum_{i=0}^r \binom{r}{i} = \sum_{i=0}^r \binom{r}{r-i} = 2^r$ ways of making the dirty parts identical. Since $n > r$, we can also make $k = n - \max(r - i, i) = \min(n - r + i, n - i)$ modifications on the clean part, unless $k > 2L - r$, in which case the number of modifications exceeds $2L - r$, the size of the clean part. Therefore, the correct upper limit for k should be $\min(2L - r, n - r + i, n - i)$. Thus, the total number of different configurations that can be obtained on the clean part is $\sum_{k=0}^{\min(2L-r, n-r+i, n-i)} \binom{2L-r}{k}$. Combining these, we obtain the contribution to $\mathcal{N}_{L,n}(r)$ for the $0 \leq r \leq n$ case:

$$\sum_{i=0}^r \sum_{k=0}^{\min(2L-r, n-r+i, n-i)} \binom{2L-r}{k} \binom{r}{i}. \quad (\text{A.5})$$

- b) $2n \geq r > n$: When $r > n$, we have to make at least $r - n$ modifications on one of the dirty parts. Therefore, the contribution to $\mathcal{N}_{L,n}(r)$ for the $2n \geq r > n$ case is

$$\sum_{i=r-n}^n \sum_{k=0}^{\min(2L-r, n-r+i, n-i)} \binom{2L-r}{k} \binom{r}{i}. \quad (\text{A.6})$$

Note that the upper limit of the first sum is not r anymore, since we are allowed to make only $n < r$ modifications in total.

- c) $r > 2n$: Since the two hyperspheres in figure A2(a) cannot overlap when $r > 2n$, the contribution to $\mathcal{N}_{L,n}(r)$ in this case is zero.

We obtain the final form of $\mathcal{N}_{L,n}(r)$ by combining equation (A.5) and equation (A.6):

$$\mathcal{N}_{L,n}(r) = \begin{cases} \sum_{i=\max(r-n,0)}^{\min(n,r)} \sum_{k=0}^{\min(2L-r, n-r+i, n-i)} \binom{2L-r}{k} \binom{r}{i} & \text{if } r \leq 2n \\ 0 & \text{otherwise} \end{cases}. \quad (\text{A.7})$$

A plot of the theoretical correlation functions for $L = 13$ with $n = 1, 2, 3, 5$, and 7 is shown in figure A1.

Appendix B. Deviations from the Theory in Correlation Functions of Highly Correlated Matrices

The theoretical calculations for the correlation function agree with the numerical results for matrices with short-range correlations. However, the numerically obtained correlation functions for highly correlated matrices differ significantly from the theory, as seen in figure 2. We here demonstrate why these deviations occur by calculating the variance of the correlated matrix elements (which is equal to the value of the correlation function at $r = 0$):

$$C(0) = \sigma_{\text{corr}}^2 = \langle (M_{ij})^2 \rangle - \langle M_{ij} \rangle^2. \quad (\text{B.1})$$

Using

$$\langle M_{ij} \rangle^2 = Z_n \langle M_{ij}^0 \rangle^2 \quad (\text{B.2})$$

(this time we do not assume $\langle M_{ij}^0 \rangle = 0$) and

$$\langle (M_{ij})^2 \rangle = \frac{1}{SZ_n} \{ (M_{00}^0)^2 + M_{00}^0 M_{01}^0 + \dots + (M_{01}^0)^2 + M_{01}^0 M_{00}^0 + M_{01}^0 M_{02}^0 + \dots \}, \quad (\text{B.3})$$

where $S = 2^{2L}$ is the total number of matrix elements, we get

$$\sigma_{\text{corr}}^2 = \frac{1}{SZ_n} \{ Z_n ((M_{00}^0)^2 + (M_{01}^0)^2 + \dots) + 2 (M_{00}^0 M_{01}^0 + \dots) \} - Z_n \langle M_{ij}^0 \rangle^2. \quad (\text{B.4})$$

Then we transform the terms in parentheses into averages and obtain

$$\sigma_{\text{corr}}^2 = \frac{1}{SZ_n} \left\{ SZ_n \langle (M_{ij}^0)^2 \rangle + \frac{2SZ_n(Z_n - 1)}{2} \langle M_{ij}^0 M_{kl}^0 \rangle_{1 \leq H(ij;kl) \leq 2n} \right\} - Z_n \langle M_{ij}^0 \rangle^2, \quad (\text{B.5})$$

which simplifies to

$$\sigma_{\text{corr}}^2 = \langle (M_{ij}^0)^2 \rangle + (Z_n - 1) \langle M_{ij}^0 M_{kl}^0 \rangle_{1 \leq H(ij;kl) \leq 2n} - Z_n \langle M_{ij}^0 \rangle^2. \quad (\text{B.6})$$

Although we intended to keep the variance of the correlated matrix elements constant through multiplication by Z_n (see equation (2)), equation (B.6) indicates that the deviations from the intended theoretical value $\sigma_0^2 = \langle (M_{ij}^0)^2 \rangle$ scale by Z_n . Our numerical studies showed that for $Z_n \gtrsim L/2$, the term $(Z_n - 1) \langle M_{ij}^0 M_{kl}^0 \rangle_{1 \leq H(ij;kl) \leq 2n} - Z_n \langle M_{ij}^0 \rangle^2$ can no longer be neglected, and deviations from the theoretical value become significant.

We verified equation (B.6) by calculating, σ_{corr}^2 , $\langle (M_{ij}^0)^2 \rangle$, $\langle M_{ij}^0 M_{kl}^0 \rangle_{1 \leq H(ij;kl) \leq 2n}$, and $\langle M_{ij}^0 \rangle^2$ in computer simulations for $L = 7$ with $n = 3$ and 4, over 100 runs each. Plugging the values for $\langle (M_{ij}^0)^2 \rangle$, $\langle M_{ij}^0 M_{kl}^0 \rangle_{1 \leq H(ij;kl) \leq 2n}$ and $\langle M_{ij}^0 \rangle^2$ obtained from the simulation into the RHS of equation (B.6) gives the same value for σ_{corr}^2 as in the simulation, with an error of $O(10^{-6})$. This result supports our theory.

Although this calculation shows the deviation only for $C(0) = \sigma_{\text{corr}}^2$, deviations for $r > 0$ should be similar due to the relatively smooth change in the overlap of the averaging hyperspheres. Since the overlaps of the averaging hyperspheres are similar for adjacent r 's, the deviations also should be similar for the adjacent $C(r)$'s. For example, the deviations at $C(0)$ and $C(1)$ should be similar in magnitude and direction. This argument explains why the numerical correlation functions look like their theoretical counterparts translated along the y axis, rather than randomly scattered around the expected data points.

- [1] Drossel B 2001 *Adv. Phys.* **50** 209 – 295
- [2] Albert R and Barabási A-L 2002 *Rev. Mod. Phys.* **74** 47–97
- [3] Drossel B and McKane A J 2002 in S Bornholdt and H G Schuster, eds, *Handbook of Graphs and Networks: From the Genome to the Internet* (Berlin: Wiley-VCH)
- [4] Dunne J, Williams R J and Martinez N D 2002 *Ecol. Lett.* **5** 558–567
- [5] Garlaschelli D, Caldarelli G and Pietronero L 2003 *Nature (London)* **423** 165–168
- [6] Garlaschelli D 2004 *Eur. Phys. J. B* **38** 277–285
- [7] Rikvold P A and Zia R K P 2003 *Phys. Rev. E* **68**(3) 011913
- [8] Zia R K P and Rikvold P A 2004 *J. Phys. A: Math. Gen.* **37**(19) 5135 – 5155
- [9] Rikvold P A 2005 in L B Kish, K Lindenberg and Z Gingl, eds, *Noise in Complex Systems and Stochastic Dynamics III* (Bellingham, WA: SPIE, The International Society for Optical Engineering) pp 148–155
- [10] Hall M, Christensen K, di Collobiano S A and Jensen H J 2002 *Phys. Rev. E* **66** 011904
- [11] Christensen K, di Collobiano S A, Hall M and Jensen H J 2002 *J. Theor. Biol.* **216**(1) 73 – 84
- [12] di Collobiano S A, Christensen K and Jensen H J 2003 *J. Phys. A* **36** 883–891
- [13] Eldredge N and Gould S J 1972 in T J M Schopf, ed, *Models In Paleobiology* (San Francisco: Freeman, Cooper) pp 82–115
- [14] Gould S J and Eldredge N 1977 *Paleobiology* **3** 115 – 151
- [15] Gould S J and Eldredge N 1993 *Nature (London)* **366** 223 – 227
- [16] Kauffman S A and Johnsen S 1991 *J. Theor. Biol.* **149**(4) 467 – 505
- [17] Kauffman S A 1993 *The Origins of Order: Self-organization and Selection in Evolution* (Oxford: Oxford University Press)
- [18] Sevim V and Rikvold P A in press in D P Landau, S P Lewis and H-B Schüttler, eds, *Computer Simulation Studies in Condensed-Matter Physics XVII*. (Berlin, Heidelberg, New York: Springer-Verlag) e-print arXiv:q-bio.PE/0403042
- [19] Shannon C E 1948 *Bell Syst. Tech. J.* **27** 379–423, 628–656 pp. 379-423 and 628-656.
- [20] Shannon C E and Weaver W 1949 *The Mathematical Theory of Communication* (Urbana: University of Illinois Press)
- [21] Krebs C J 1989 *Ecological Methodology* (New York: Harper & Row) chap. 10
- [22] The PSD of a variable $y(t)$, where t takes N discrete values with an increment Δ , is here defined as $Y(f) = (\Delta/N) |\sum_i [y(t) - \bar{y}] \exp(2\pi i f t)|^2$, where \bar{y} is the average of $y(t)$ and $f = n/(N\Delta)$ with $n = -N/2, \dots, N/2$. It was calculated with subroutine `spctrm` from Ref. [23], using a Welch window and variance reduction as described there.
- [23] Press W H, Teukolsky S A, Vetterling W T and Flannery B P 1992 *Numerical Recipes, Second Ed.* (Cambridge: Cambridge University Press)